



Synthesis of bimetallic PdAu nanoparticles for formic acid oxidation

Yange Suo, I-Ming Hsing*

Department of Chemical and Biomolecular Engineering, The Hong Kong University of Science and Technology, Clear Water Bay, Kowloon, Hong Kong SAR, China

ARTICLE INFO

Article history:

Received 14 October 2010

Received in revised form 9 December 2010

Accepted 9 December 2010

Available online 16 December 2010

Keywords:

Ethylene glycol

Alloy

Non-alloy

Lattice parameter

ABSTRACT

In this work, a simple co-deposition strategy for the synthesis of carbon-supported Pd–Au alloy was reported. Our approach involves the co-reduction of Au and Pd ions using ethylene glycol and sodium citrate as the reducing and stabilizing reagents. Both alloy and non-alloy bimetallic Pd–Au nanoparticles are produced using a right rate-limiting strategy. For example, when ethylene glycol and sodium citrate are the limiting reagent with Au and Pd ions in excess, the synthesis environment favors preferential nucleation and growth of Au nanoparticles followed by deposition of Pd either as the shell of Au core or as separate Pd clusters. On the other hand, if the supply of metal ions (not the reducing reagents) limits the reaction, it creates a synthesis condition for Pd–Au alloy particles. The as-prepared Pd–Au alloys exhibit higher Pd-specific activities towards formic acid oxidation compared with the non-alloy counterpart or individual Pd catalyst and an easier removal of adsorbed oxygen species (e.g., O_{ads} or OH_{ads}) was observed from the surface of Pd–Au alloy with a higher content of Au.

© 2010 Elsevier Ltd. All rights reserved.

1. Introduction

Structural or electronic properties of binary catalysts could be very different from that of their individual components and enhanced activity or stability of the binary catalysts were often observed [1,2]. Among the various bimetallic materials, Pd–Au system is an interesting one as it shows high activity towards useful chemical reactions (e.g., hydrogenation of 4-pentenotic acid [3], acetoxylation of ethylene to vinyl acetate [4], and oxidation of alcohols to aldehydes [5]) as well as electrochemical reactions (e.g., ethanol oxidation [6], 2-propanol oxidation [7], and formic acid oxidation [8]). Investigations of catalysts for formic acid electro-oxidation have attracted interests due to their use in direct formic acid fuel cell, a promising power device for consumer electronics. Au_{core} – Pd_{shell} structured materials have been reported to show enhanced activity for formic acid oxidation than the well-known Pd [8,9]. Catalytic properties of bimetallic nanoscale catalysts are highly dependent on their structure (e.g., alloy, core–shell structure) and surface composition [10]. Moreover, interesting and unique electrochemical properties of Pd–Au alloys for formic acid oxidation might be explored.

Although efforts have been made to study the synthesis of Pd–Au bimetallic nanocatalysts, preparation of alloy structured Pd–Au nanoparticles is still considered to be a big challenge [11,12]. The synthesis of core–shell structured Pd–Au catalysts can be easily achieved using either sequential [13,14] or co-reduction methods [11,12,15]. To make alloy catalysts, Ksar et al. [6] have reported a

radiolytic reduction method, through which, Pd–Au alloy nanoparticles stabilized by poly(acrylic acid) were achieved. Mejía-Rosales et al. [16] synthesized and characterized Pd–Au nanoparticles passivated with poly(vinylpyrrolidone) (PVP) using a sequential reduction protocol. Using hydrazine as the strong reductant, PVP-protected Pd–Au alloy nanodendrites with an average particle size of 15–26 nm have been synthesized [17].

In this work, we report a simple co-reduction method with ethylene glycol and sodium citrate as the reducing and stabilizing agents to synthesize Pd–Au bimetallic nanoparticles. Traditionally, the formation of Pd–Au alloys through concurrent reduction of Pd and Au ions is not easy because of the vast difference of redox potentials between Au and Pd [15]. At the same reducing environment, Au ions have much higher reduction rate than that of Pd ions. To overcome this limitation, our approach adopts the principle of reaction engineering and rate-limiting strategy to carefully control the synthesis environment that would enable the production of alloy and non-alloy Pd–Au bimetallic nanoparticles. Pd–Au alloy nanoparticles with different metallic compositions were successfully synthesized by this new approach. Electrochemical evaluation suggests that the as-synthesized Pd–Au alloys exhibit higher Pd-specific activities towards formic acid electro-oxidation than Pd/C. Moreover, Pd–Au catalysts consisting of a higher content of Au show an easier removal of adsorbed oxygen species (e.g., O_{ads} or OH_{ads}).

2. Experimental

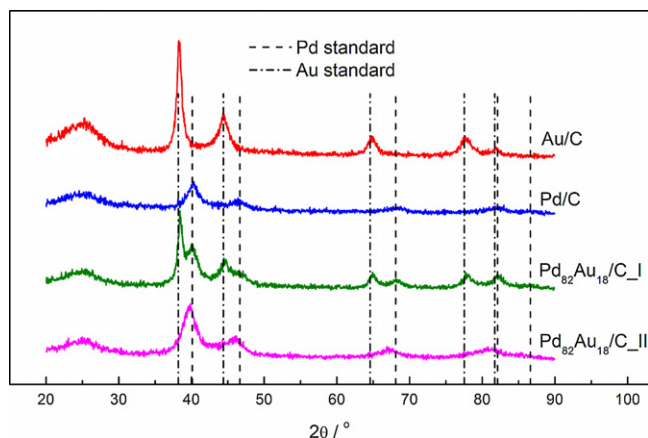
2.1. Chemicals

Ammonium tetrachloropalladate ($(NH_4)_2PdCl_4$, 99.995%), hydrogen tetrachloroaurate trihydrate ($HAuCl_4 \cdot 3H_2O$, 99.9%),

* Corresponding author. Tel.: +852 23587131; fax: +852 31064857.
E-mail address: kehsing@ust.hk (I-M. Hsing).

Table 1
Metallic loadings of catalysts based on ICP-AES characterization.

Catalysts	Metallic loadings based on ICP-AES characterization (%)		Atomic ratio (Pd/Au)	
	Au	Pd	Experimental	Precursor
Pd	N/A	12.7	N/A	N/A
Pd ₈₂ Au ₁₈ /C.I	4.8	10.9	81/19	82/18
Pd ₈₂ Au ₁₈ /C.II	4.9	12.8	83/17	82/18
Pd ₆₇ Au ₃₃ /C.II	8.1	8.8	67/33	67/33
Pd ₅₀ Au ₅₀ /C.II	10.3	5.9	51/49	50/50

**Fig. 1.** XRD patterns of Au/C, Pd/C, and Pd₈₂Au₁₈/C (prepared by protocols I and II) catalysts.**Table 2**
Crystal size and lattice parameter of the Pd/C, Au/C and Pd₈₂Au₁₈/C (prepared by protocols I and II) based on XRD characterization.

Catalysts	Crystal size/nm	Lattice parameter/nm
Pd/C (protocol II)	3.6	0.3893
Au/C (protocol II)	7.2	0.4064
Pd ₈₂ Au ₁₈ /C (protocol I)	4.2 (Pd)	0.3890 (Pd)
	6.8 (Au)	0.4054 (Au)
Pd ₈₂ Au ₁₈ /C (protocol II)	3.0	0.3940

ethylene glycol (C₂H₆O₂, 99.5%), perchloric acid (HClO₄, 69%) were purchased from Sigma Aldrich. Sodium citrate (C₆H₅Na₃O₇·2H₂O, 99%) was ordered from BDH. Formic acid (HCOOH, 98%) was ordered from Riedel-de-Haën. Vulcan XC-72 carbon was purchased from E-TEK. Nafion solution (5%) was received from Dupont. Ethanol (C₂H₅OH, 99.5%) was purchased from Merck KGaA.

2.2. Synthesis of catalysts

2.2.1. Synthesis protocol I for Pd₈₂Au₁₈/C catalyst

Firstly, 21.9 mg ammonium tetrachloropalladate ((NH₄)₂PdCl₄) and 0.65 ml hydrogen tetrachloroaurate trihydrate (HAuCl₄·3H₂O) aqueous solution (1 g/100 ml) were dissolved into 48 ml water

Table 3
Atomic compositions of five nanoparticles of the Pd₈₂Au₁₈/C.II catalyst based on EDX characterization.

Nanoparticles	Pd (atom %)	Au (atom %)
# 1	89.30	10.70
# 2	85.81	14.19
# 3	82.38	17.62
# 4	86.35	13.65
# 5	88.50	11.50
Stoichiometric value	82	18

Table 4
Atomic compositions of five nanoparticles of the Pd₈₂Au₁₈/C.I catalyst based on EDX characterization.

Nanoparticles	Pd (atom %)	Au (atom %)
# 1	100	N/A
# 2	87	13
# 3	57	43
# 4	100	N/A
# 5	100	N/A
Stoichiometric value	82	18

to obtain the precursor solution. Then, 48 mg Vulcan XC-72 carbon was poured into the solution to get the precursor suspension, which was stirred and ultrasonically mixed for 2 h. At the same time, 0.283 g sodium citrate was dissolved into 2 ml water + 10 ml ethylene glycol mixture solution to get the sodium citrate water/ethylene glycol solution. After removing air with Ar gas bubbling for 30 min, the precursor suspension was refluxed at 170 °C oil bath for 5 min and then the prepared sodium citrate water/ethylene glycol solution was added into the heated precursor suspension drop by drop. Another 40 ml ethylene glycol was added into the reaction system, which was then continued to be heated for another 2 h. The reaction product was filtered and washed with water and ethanol. The residue was dried at 60 °C oven for 12 h and then grounded in an agate mortar. Catalyst synthesized by this protocol is denoted as Pd₈₂Au₁₈/C.I in the following discussion.

2.2.2. Synthesis protocol II for Pd₈₂Au₁₈/C catalyst

Firstly, 0.283 g sodium citrate was dissolved into 50 ml water/ethylene glycol mixture solution (volume/volume = 1:1), and then 48 mg Vulcan XC-72 carbon was poured into the above solution to obtain the sodium citrate suspension, which was stirred and ultrasonically mixed for 2 h. At the same time, 21.9 mg ammonium tetrachloropalladate ((NH₄)₂PdCl₄) and 0.65 ml hydrogen tetrachloroaurate trihydrate (HAuCl₄·3H₂O) aqueous solution (1 g/100 ml) were dissolved into another 10 ml water/ethylene glycol solution (volume/volume = 1:1) to obtain the precursor solution. After removing air with Ar gas bubbling for 30 min, the sodium citrate suspension was refluxed at 170 °C oil bath. After 5 min heating, the precursor solution was added into the heated sodium citrate suspension drop by drop. Another 40 ml water/ethylene glycol solution (volume/volume = 1:1) was added into the reaction system, which was then continued to be heated for another 2 h. The reaction product was filtered and washed with water and ethanol. The residue was dried at 60 °C for 12 h and then grounded in an agate mortar. Catalyst synthesized by this protocol is denoted as Pd₈₂Au₁₈/C.II in the following discussion.

Protocol II was also used for the synthesis of Pd/C (same palladium/carbon ratio with that in the Pd₈₂Au₁₈/C catalysts), Au/C (same gold/carbon ratio with that in the Pd₈₂Au₁₈/C catalysts), Pd₆₇Au₃₃/C (metal loading of 20 wt% with atomic ratio of Pd to Au being 67:33 in the precursor solution) and Pd₅₀Au₅₀/C (metal loading of 20 wt% with atomic ratio of Pd to Au being 50:50 in the precursor solution).

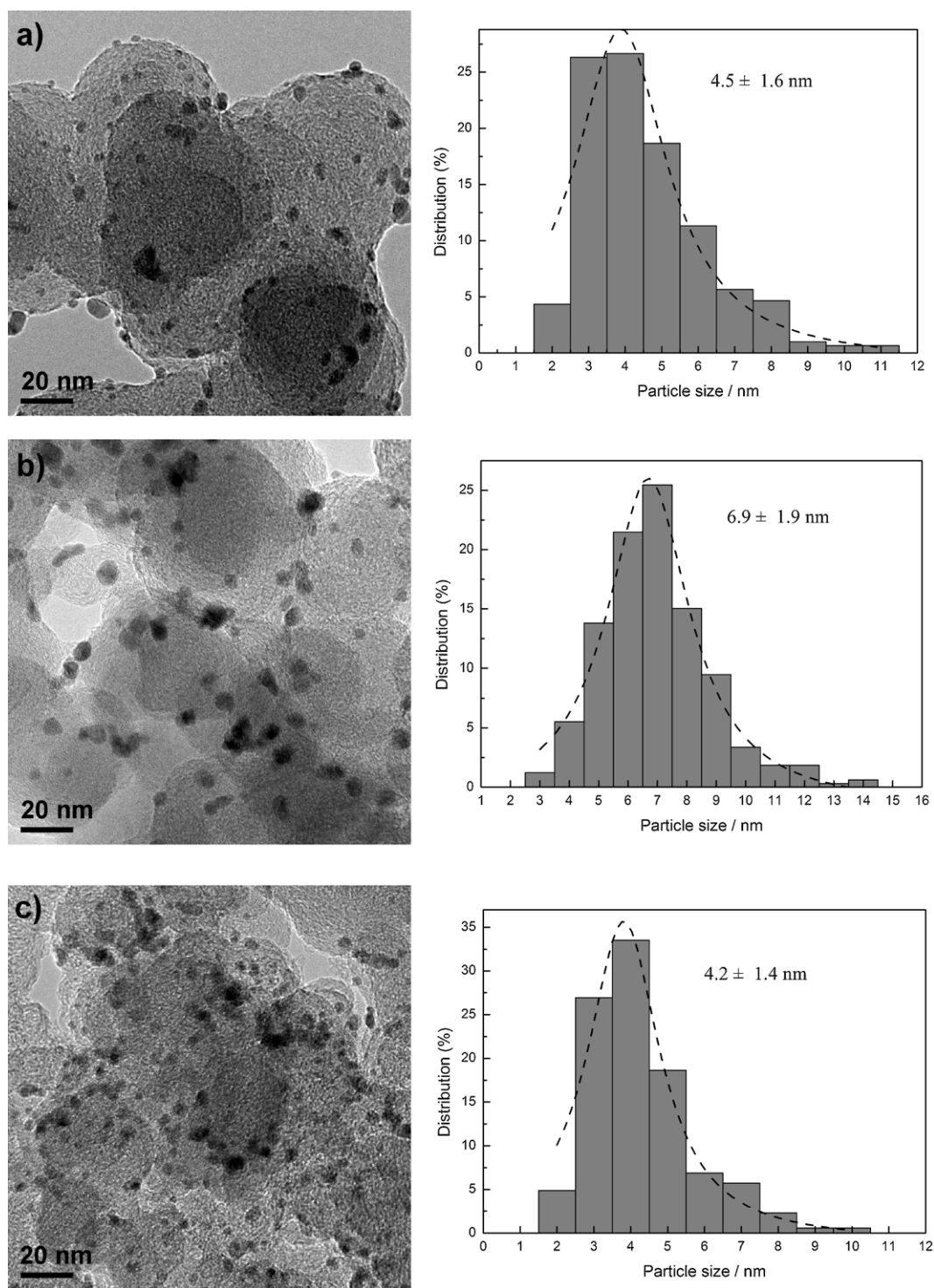


Fig. 2. TEM images and the size distribution of (a) Pd/C, (b) Pd₈₂Au₁₈/C.I and (c) Pd₈₂Au₁₈/C.II catalysts.

2.3. Physicochemical characterization

Inductively coupled plasma atomic emission spectroscopy (ICP-AES) was carried out using an Optima 3000XL system (Perkin Elmer) to measure the real metallic loadings of the catalysts. The following procedure was followed to prepare the samples. Firstly, 5 mg catalyst was poured into 50 ml aqua regia and the mixture was left at room temperature for 42 h to completely dissolve metallic nanoparticles. The obtained suspension was then centrifuged with a rotating rate of 13,400 rpm for 2 min. The supernatant was taken out and then diluted to do ICP-AES characterization.

Powder X-ray diffraction (XRD) was carried out with a PANalytical X-ray diffractometer (Model X'pert Pro) using a Cu K α radiation source operating at 40 kV and 40 mA. For crystalline size and lattice parameter analysis, (2 2 0) diffraction peak was fitted to a Lorentzian line shape to obtain the values of diffraction angle and breadth of diffraction line at half-maximum intensity.

Transmission electron microscopy (TEM) was carried out with a JEOL 2010F high resolution TEM system operated with LaB₆ filament at 200 kV. The samples were prepared by dropping catalyst suspensions (prepared by dispersing the catalysts ultrasonically in ethanol) onto carbon coated Cu grids and then dried at room tem-

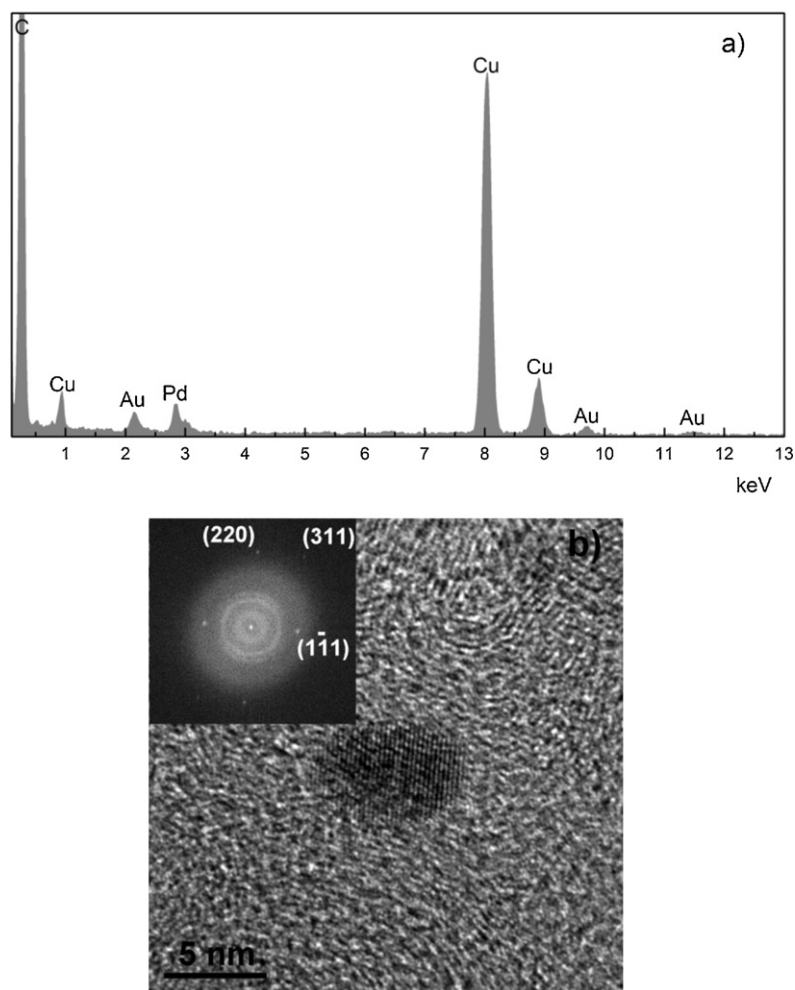


Fig. 3. (a) EDX spectrum of one nanoparticle of the Pd₈₂Au₁₈/C.II catalyst and (b) HRTEM image of one nanoparticle of the Pd₈₂Au₁₈/C.II catalyst and the inset picture is the corresponding Fast Fourier Transfer (FFT) image.

perature. Number average particle size was recorded by taking the size average of more than 300 particles. Atomic percentages of Pd and Au were measured by energy-dispersive X-ray spectroscopy (EDX), which was integrated with TEM equipment. To get rid of contamination by other nanoparticles, we chose single particles which are not closely surrounded by other metallic nanoparticles. The spot size of the light beam for EDX analysis was a few nanometers.

X-ray photoelectron spectroscopy (XPS) was carried out with a Physical Electronics PHI 5600 multi-technique system, using Al monochromatic X-ray at a power of 350 W.

2.4. Electrochemical evaluation

Electrochemical measurements were carried out using an Autolab potentiostat (PGSTAT20, Eco Chemie, The Netherlands) in a conventional three-electrode cell with a catalyst coated glassy carbon electrode (working electrode), a Pt coil (counter electrode) and a saturated Ag/AgCl electrode (reference electrode). All the potentials in our data are converted to be referred to standard hydrogen electrode (SHE). The glassy carbon substrate was polished with alumina suspension prior to use. To prepare the working electrode, 7 mg catalyst was dispersed ultrasonically in 1 ml diluted nafion solution (0.05 wt% in ethanol) for 30 min and 10 μ l of the suspension was pipetted onto the glassy carbon electrode ($d=5$ mm) by a microsyringe and left to dry at room temperature. Prior to

the activity measurement, the working electrode was cleaned by CV sweeping in Ar-saturated 1 M HClO₄ solution. Then a certain amount (in order to keep the concentration in the electrolyte as 1 M) of formic acid was added into the electrolyte to do the activity measurements. Pd-specific activities were obtained through normalizing formic acid oxidation currents with the electrochemical active surface area of Pd, measured by analyzing the Pd surface oxide reduction and CO stripping charge. As the peak area of the surface oxide reduction in the cyclic voltammogram (CV) is proportional to the electrochemical surface area of the catalyst, peak areas of Pd surface oxide reduction were simply used to denote the electrochemical surface areas. Pd-specific activities were obtained by simply normalizing formic acid oxidation currents with the peak areas of the Pd surface oxide reduction (potential range of CV scan: 0.06–1.16 V) of the catalysts in Ar saturated 1 M HClO₄. The unit of Pd-specific activities obtained by this method is not mA cm⁻², but denoted as arbitrary unit (a.u.) The quantified Pd active surface areas of the catalysts were measured by CO stripping experiments and the following procedures were followed. Firstly, the working electrode was cleaned by CV sweeping in Ar saturated 1 M HClO₄ solution. CO gas was then bubbled into the electrolyte solution for 20 min. The working electrode was held at 0.1 V for 15 min for CO adsorption. Ar gas was then bubbled into the electrolyte for 30 min to remove excess CO dissolved in the solution. CV sweeping was conducted to do CO stripping. The active surface areas were obtained by calculating

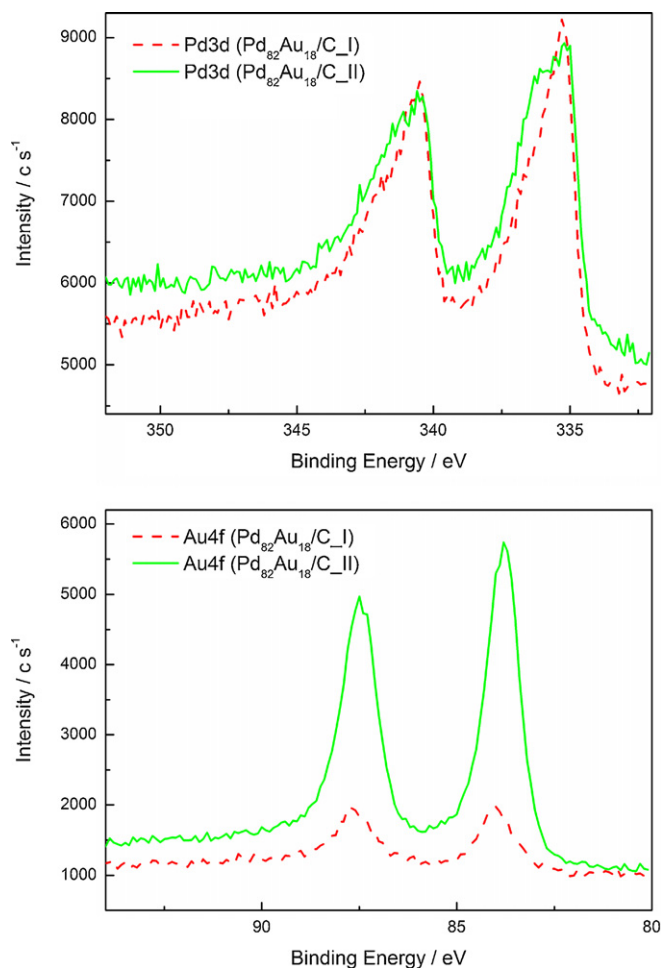
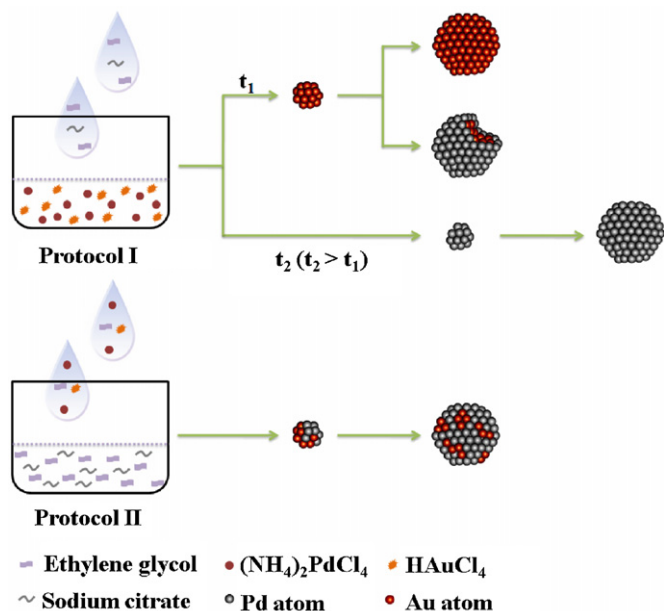


Fig. 4. XPS spectra of Pd3d and Au4f of Pd₈₂Au₁₈/C catalysts (prepared by protocols I and II).



Scheme 1. Illustration of two protocols for the preparation of bimetallic Pd–Au catalysts supported on carbon. Protocol I: drop by drop addition of ethylene glycol and sodium citrate (the reducing and stabilizing reagents) to the abundant mixture of metallic precursors; protocol II: drop by drop addition of the Pd and Au ion precursors to the abundant mixture of ethylene glycol and sodium citrate.

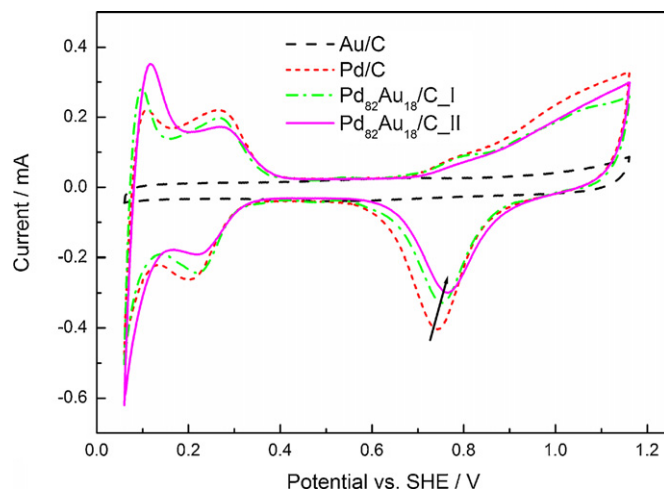


Fig. 5. Cyclic voltammograms of Au/C, Pd/C and Pd₈₂Au₁₈/C (prepared by protocols I and II) catalysts in Ar-saturated 1 M HClO₄ solution at room temperature with scan rate of 50 mV/s.

the stripping charges of pre-adsorbed CO (assuming 420 $\mu\text{C cm}^{-2}$). Through normalizing formic acid oxidation currents by the active surface areas, the Pd-specific activities were then obtained. All electrochemical experiments were conducted at room temperature.

3. Results and discussion

3.1. Synthesis of Pd–Au bimetallic catalysts

ICP-AES was carried out to analyze the real metallic loadings of the Pd₈₂Au₁₈/C and Pd/C catalysts. As shown in Table 1, the measured atomic ratios of Pd to Au in Pd₈₂Au₁₈ catalysts are consistent with the stoichiometric value (82:18) in the precursor solution.

XRD patterns of the Pd/C, Au/C and bimetallic Pd₈₂Au₁₈/C catalysts are shown in Fig. 1. Positions of the diffraction peaks of Pd/C and Au/C catalysts fit well with their characteristic face centered cubic (fcc) patterns. Pd₈₂Au₁₈/C.I exhibits XRD patterns with superimposed patterns of Pd/C and Au/C, suggesting a structure of non-alloy catalysts. This result is consistent with the literature report of Pd–Au catalyst prepared with microwave-assisted synthesis protocol using ethylene glycol as the reducing reagent [11]. On the other hand, Pd₈₂Au₁₈/C.II reveals new diffraction peaks with positions between that of pure Pd/C and Au/C. The lattice parameter, calculated based on Bragg's law [18] using (220) diffraction peak (at 67.15°), is 0.3940 nm (Table 2), which is similar to the empirical value of Pd₈₂Au₁₈ (0.3924 nm) by Vegard's law [19]. XRD data suggests that the bimetallic Pd–Au particles by protocol II could form an alloy structure.

TEM images of the Pd/C, Pd₈₂Au₁₈/C.I and Pd₈₂Au₁₈/C.II catalysts indicate that all the catalysts are well dispersed on the carbon surface (Fig. 2). The histogram of particle size distribution of each catalyst was obtained by recording more than 300 nanoparticles at different areas. The average particle size of Pd₈₂Au₁₈/C.II (4.2 nm) is close to that of Pd/C (4.5 nm). Pd₈₂Au₁₈/C.I exhibits a larger average size of 6.9 nm.

EDX spectrum (Fig. 3a) of one particle of the Pd₈₂Au₁₈/C.II catalyst shows that a single particle is composed of both Pd and Au elements. Moreover, atomic compositions of the five nanoparticles are roughly consistent with the stoichiometric value (Table 3). Fig. 3b shows the high resolution TEM (HRTEM) image of one specific particle of the Pd₈₂Au₁₈/C.II catalyst and the inset photo shows its corresponding Fast Fourier Transfer (FFT) image. Three groups of diffraction spots are observed. By measuring the distance between

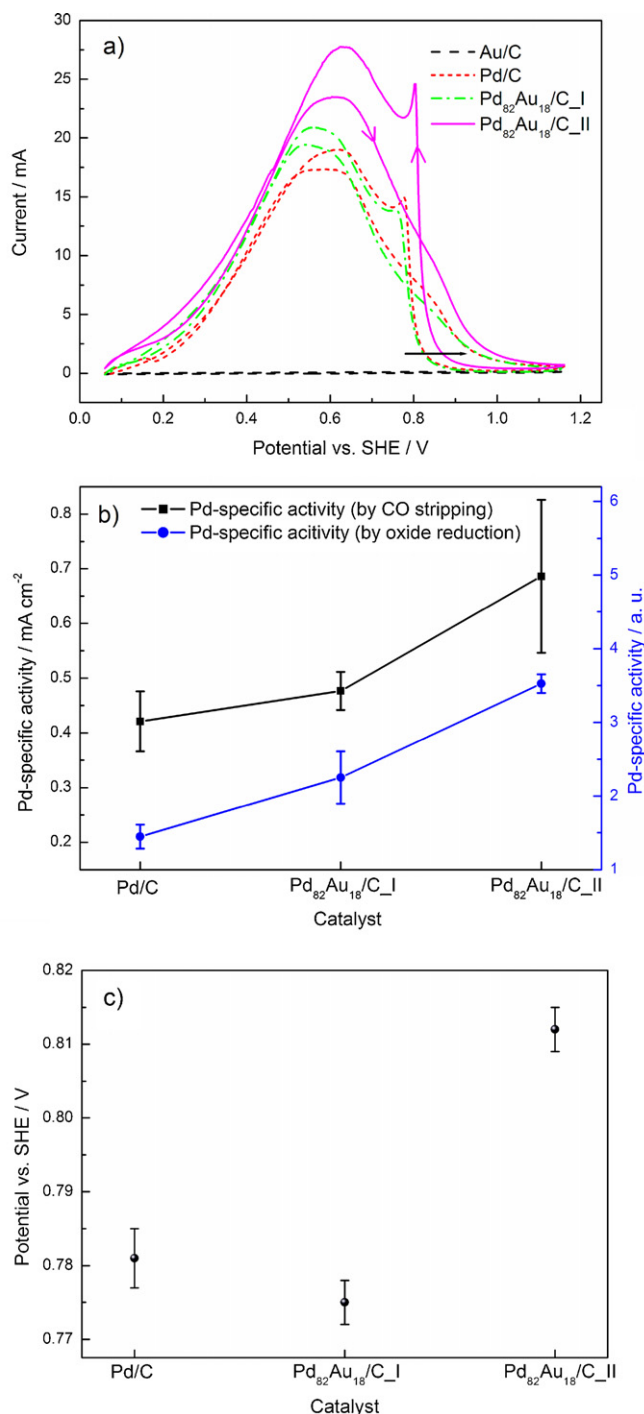


Fig. 6. (a) Cyclic voltammogram of Au/C, Pd/C and Pd₈₂Au₁₈/C (prepared by protocols I and II) catalysts in Ar-saturated 1 M HCOOH + 1 M HClO₄ at room temperature with scan rate of 50 mV/s, (b) Pd-specific activities (through normalizing formic acid oxidation currents by the electrochemical active surface areas of Pd) at 0.2 V on Pd/C and Pd₈₂Au₁₈/C (prepared by protocols I and II) and (c) potentials (averaged by three measurements) of the abrupt current increase in the backward sweep on Pd/C and Pd₈₂Au₁₈/C (prepared by protocols I and II).

the two spots in each group, the inter-planer distances of 0.226 nm, 0.140 nm and 0.120 nm are obtained. The measured values are consistent with the empirical values of Pd₈₂Au₁₈ (1 1 1), (2 2 0), (3 1 1) crystallographic planes, which are 0.227 nm, 0.139 nm and 0.118 nm respectively based on Vegard's law [19]. EDX and high resolution TEM image confirm that Pd₈₂Au₁₈/C_II form an alloy structure. Unlike that of Pd₈₂Au₁₈/C_II, atomic compositions based

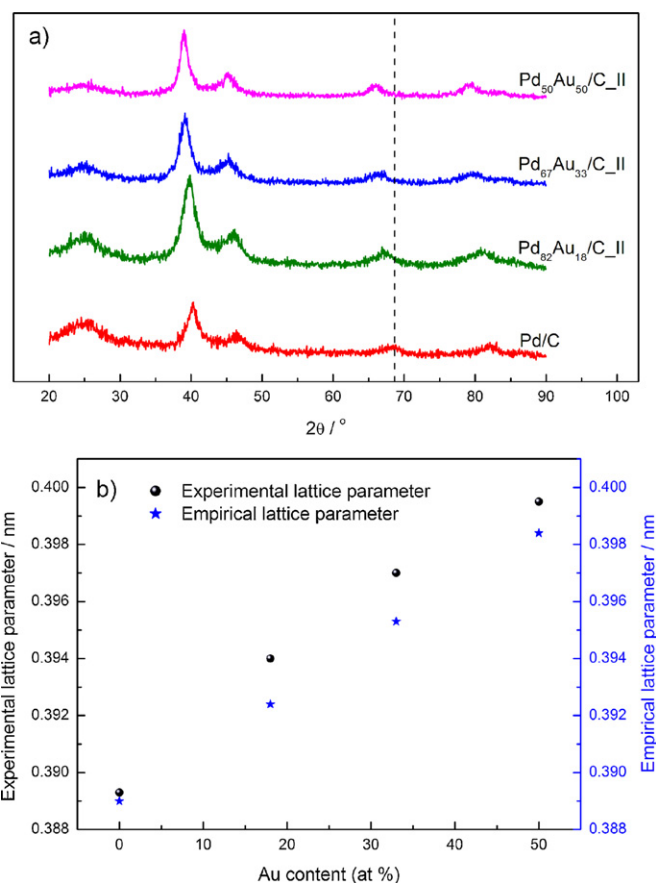


Fig. 7. (a) XRD patterns of the Pd–Au/C catalysts with different metallic compositions synthesized by protocol II and (b) comparison of the experimental and empirical lattice parameters of the carbon supported Pd–Au alloys with different metallic compositions synthesized by protocol II.

on EDX spectrum of five nanoparticles of the Pd₈₂Au₁₈/C_I suggest that there are individual Pd and Pd–Au bimetallic nanoparticles (Table 4) in the catalyst.

XPS characterization was carried out to get surface information. Fig. 4 shows the Pd3d and Au4f peaks of the Pd₈₂Au₁₈/C_I and Pd₈₂Au₁₈/C_II catalysts. Surface atomic ratio of Pd to Au in Pd₈₂Au₁₈/C_I is 93:7, which is much larger than the stoichiometric value (82:18), indicating enrichment of Pd element on the surface of the nanoparticles. On the contrary, surface atomic ratio of Pd to Au in Pd₈₂Au₁₈/C_II is 77:23, which is close to the stoichiometric value (82:18).

The above results have strongly suggested that most of the Pd–Au nanoparticles in Pd₈₂Au₁₈/C_II catalyst form alloy structure, while non alloy nanoparticles are generated using protocol I. As illustrated in Scheme 1, when the rate-limiting reactant (supplied in drop-by-drop) of the reducing agent (ethylene glycol and sodium citrate) is added to the metallic ion solutions in excess, it creates a synthesis environment for faster deposition of Au than Pd due to higher reduction potential of Au ions than that of Pd ions [20] and thus leads to core–shell, as well as other non-alloy structure of Pd–Au. On the other hand, the environment of a limited supply of Pd and Au ion precursors (supplied in drop-by-drop) and an abundant amount of reducing reagents at high temperature, as shown in protocol II, accelerates the reduction rates of both Pd and Au ions and drives the synthesis process to be controlled by the mass transport of ion reactants (i.e., Pd and Au precursors). Therefore, the drop-by-drop arrival of Pd and Au ions determines catalyst synthesis condition and simultaneous reduction of Pd and Au ions to form alloy structure is thus achievable.

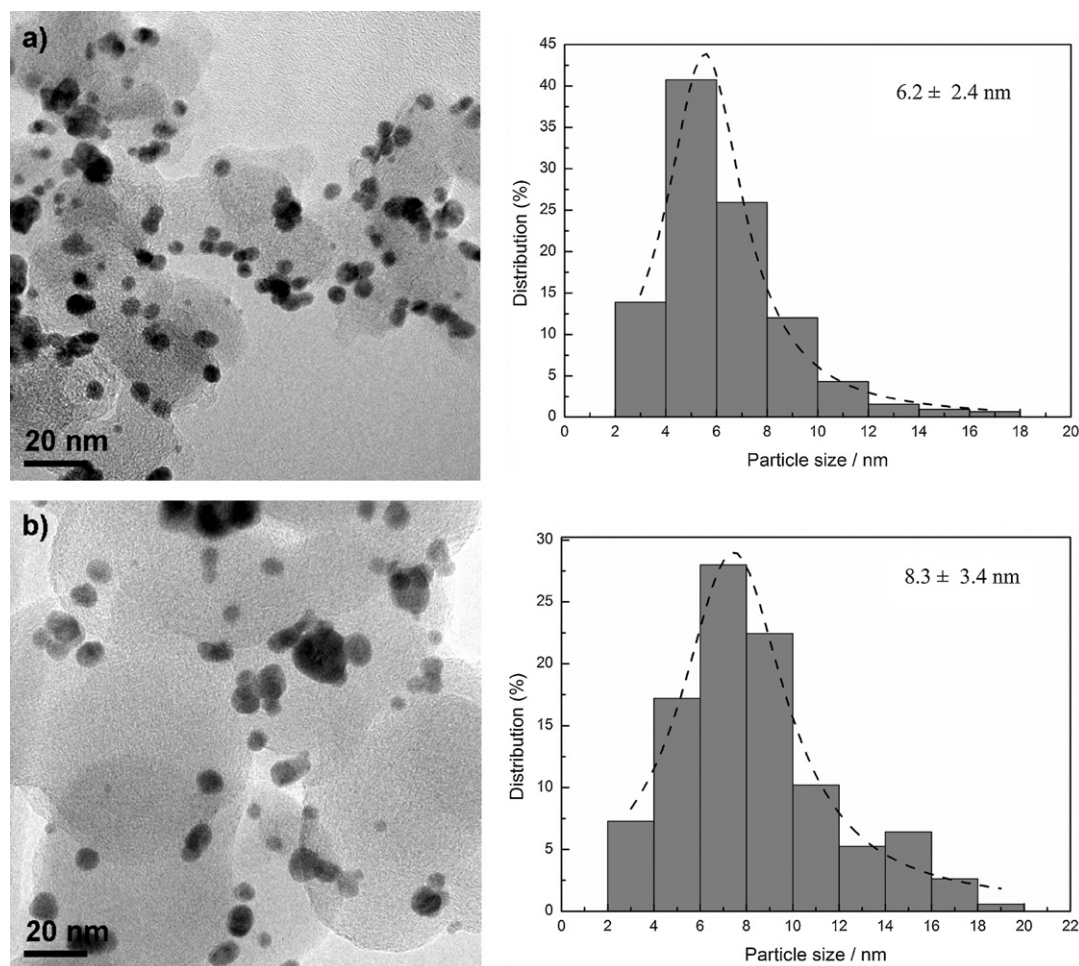


Fig. 8. TEM images and the size distribution of (a) Pd₆₇Au₃₃/C.II and (b) Pd₅₀Au₅₀/C.II.

3.2. Electrochemical properties of Pd₈₂Au₁₈/C catalyst in comparison with Pd/C and Au/C

Cyclic voltammetric investigations of binary Pd₈₂Au₁₈/C prepared by protocols I and II in benchmark comparison with Au/C and Pd/C are reported in Figs. 5 and 6a. Other than Au/C, Pd/C and Pd₈₂Au₁₈/C catalysts exhibit high surface reaction currents in the measured potential range (Fig. 5). Current peaks of hydrogen desorption/adsorption at low potentials (i.e., 0.06–0.4 V), and surface oxidation/reduction at high potentials (i.e., higher than 0.6 V) reveal typical CV characteristics of a “palladium-like” catalyst. Moreover, the reduction peak of surface oxide reveals an anodic shift on the Pd₈₂Au₁₈/C catalyst compared with that on Pd/C. Pd₈₂Au₁₈/C.II, in particular, shows the highest shift (as indicated by the arrow in Fig. 5), indicating an easier removal of adsorbed oxygen species

from Pd₈₂Au₁₈/C alloy catalyst compared with that from non-alloy counterpart or Pd/C. Size and electronic effects could lead to the phenomenon of this easier removal of adsorbed oxygen species from the substrate. On larger particles, easier removal of adsorbed oxygen species from Pt or Pd surface was observed [21,22]. However, based on previous XRD and TEM analysis (Table 2 and Fig. 2), Pd₈₂Au₁₈/C.II has a relatively smaller particle size compared with Pd₈₂Au₁₈/C.I or Pd/C. Therefore, the observed phenomenon of easier removal of adsorbed oxygen species from Pd₈₂Au₁₈/C.II compared with that from Pd₈₂Au₁₈/C.I or Pd could not be explained by the particle size effect.

Fig. 6a shows the polarization curves of formic acid oxidation on Au/C, Pd/C and Pd₈₂Au₁₈/C catalysts. Au/C shows no catalytic activity for formic acid oxidation in the measured potential range. The activity of Pd₈₂Au₁₈/C is higher than that of Pd/C, with Pd₈₂Au₁₈/C.II

Table 5

Atomic compositions of five nanoparticles of the Pd₆₇Au₃₃/C.II catalyst based on EDX characterization.

Nanoparticles	Pd (atom %)	Au (atom %)
# 1	91.27	8.73
# 2	76.55	23.45
# 3	69.88	30.12
# 4	61.89	38.11
# 5	66.70	33.30
Stoichiometric value	67	33

Table 6

Atomic compositions of five nanoparticles of the Pd₅₀Au₅₀/C.II catalyst based on EDX characterization.

Nanoparticles	Pd (atom %)	Au (atom %)
# 1	53.90	46.10
# 2	56.07	43.93
# 3	56.73	43.27
# 4	56.43	43.57
# 5	71.88	28.12
Stoichiometric value	50	50

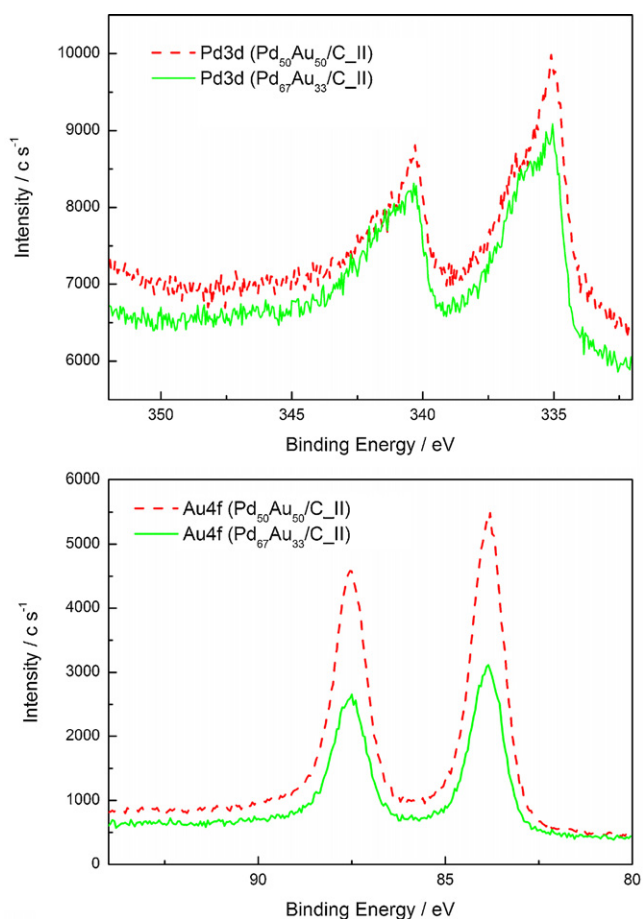


Fig. 9. XPS spectra of Pd3d and Au4f of the Pd₆₇Au₃₃/C.II and Pd₅₀Au₅₀/C.II.

exhibiting the highest activity. Fig. 6b shows the Pd-specific activities at 0.2 V on different catalysts. It can be seen that Pd₈₂Au₁₈/C.II shows a higher activity compared with Pd₈₂Au₁₈/C.I and Pd/C. In addition, the sharp increase of the current during the backward scan on the Pd₈₂Au₁₈/C.II occurs at a more positive potential (as indicated by the arrow sign) than that of the other catalysts (Fig. 6a and c). As discussed in our previous work [22], the adsorbed oxygen species could block the active surface area of Pd. Removal of these adsorbed oxygen species could trigger a sharp current increase during the backward sweep. Therefore, consistent with the CV results shown in Fig. 5, an anodic shift of sharp current increase on Pd₈₂Au₁₈/C.II catalyst suggests that it is easier to remove adsorbed oxygen species from carbon supported Pd–Au alloy surface than that from the non-alloy counterpart or single Pd surface. Interestingly, Pt surface has also been reported to become more resistant towards surface oxidized species formation through manipulation by small Au clusters [1]. The d-band theory proposed by Hammer and Nørskov [23] provides a theoretical analysis for estimation of surface reactivity. Based on their model, the surface reactivity is related to the position of the center of metal d-band. Shift of d-band center has been demonstrated for Pd overlayers on Au and Au overlayers on Pd compared with pure Au or Pd substrates by theoretical calculation [24]. Therefore, the observed phenomenon of easier removal of adsorbed oxygen species from carbon supported Pd–Au alloy in comparison with that from non-alloy counterpart or carbon supported Pd in this work could be caused by the adjusted electronic properties due to alloying Au to Pd.

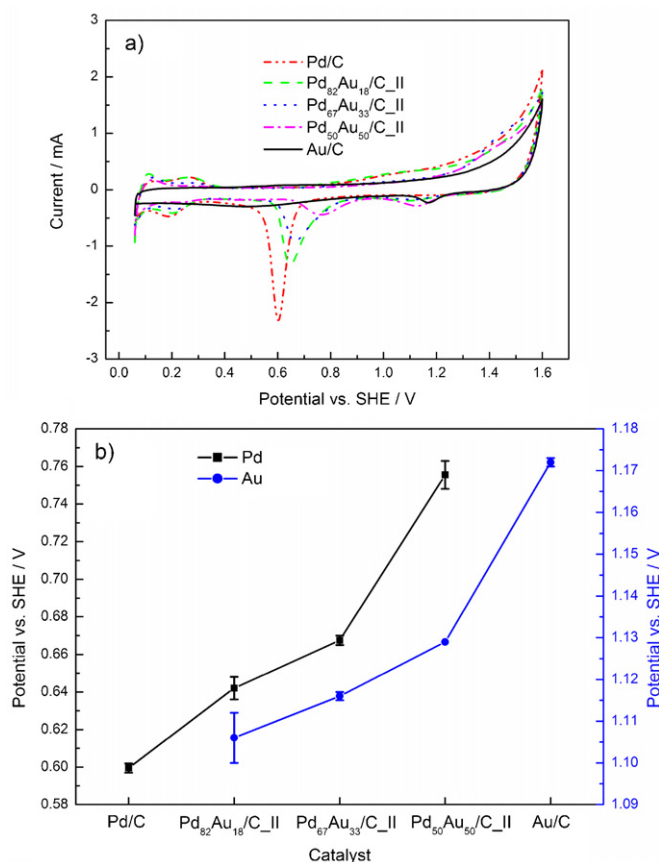


Fig. 10. (a) Cyclic voltammogram of Au/C, Pd/C and Pd–Au/C catalysts with different metallic compositions synthesized by protocol II in Ar-saturated 1 M HCOOH at room temperature with scan rate of 50 mV/s and (b) peak potentials of the surface oxide reduction of the Au/C, Pd/C and Pd–Au/C catalysts with different metallic compositions synthesized by protocol II.

3.3. Effect of metallic composition on the electrochemical property of Pd–Au/C

Pd–Au/C catalysts with other metallic compositions (Pd₆₇Au₃₃/C, Pd₅₀Au₅₀/C) were also synthesized using our protocol II. The metallic loadings of the Pd–Au/C catalysts were characterized by ICP-AES. The metallic ratios of Pd to Au are consistent with that in the precursor solutions, as shown in Table 1.

XRD patterns of the Pd–Au/C catalysts with different metallic compositions synthesized by protocol II are compared with that of Pd/C (Fig. 7a). All the Pd–Au/C catalysts exhibit characteristic fcc diffraction peaks with positions between that of Pd/C and Au/C, indicating the formation of alloy structures. The corresponding diffraction peaks shift towards lower diffraction angles with the increase of Au content. Fig. 7b shows experimental lattice parameters (calculated based on Bragg's law [18] using (2 2 0) diffraction peak) and empirical lattice parameters (based on Vegard's law [19]) of the catalysts with different metallic compositions. Clearly, the experimental lattice parameters are consistent with the empirical values and with the increase of Au content, lattice parameter of the Pd–Au catalyst increases.

Nanoparticles in Pd₆₇Au₃₃/C.II and Pd₅₀Au₅₀/C.II catalysts are well dispersed on carbon surface, as shown in TEM images (Fig. 8). However, a wide size distribution is observed. With the increase of Au content, the average particle size of the Pd–Au catalysts increases. Atomic compositions (measured by EDX) of five single particles in Pd₆₇Au₃₃/C.II and Pd₅₀Au₅₀/C.II catalysts are consistent with their stoichiometric values (Tables 5 and 6).

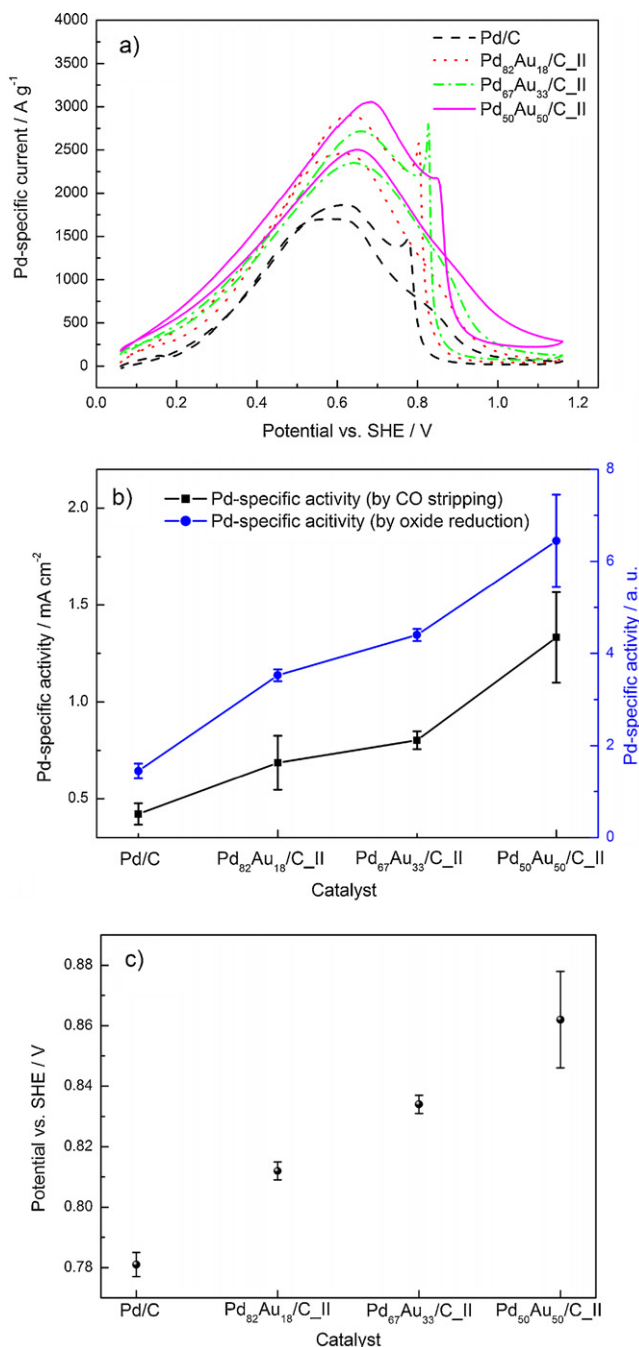


Fig. 11. (a) Polarization curves (currents normalized by Pd contents based on ICP-AES characterization) of 1 M formic acid oxidation on Pd–Au/C alloys with different metallic compositions synthesized by protocol II in Ar-saturated 1 M HClO₄ solution at room temperature with scan rate of 50 mV/s, (b) Pd-specific activities (through normalizing formic acid oxidation currents by the electrochemical active surface areas of Pd) at 0.2 V on Pd–Au/C catalysts with different metallic compositions synthesized by protocol II and (c) potentials (averaged by three measurements) of the abrupt current increase in the backward sweep on Pd–Au/C catalysts with different metallic compositions synthesized by protocol II.

Fig. 9 shows the Pd3d and Au4f XPS spectra of the Pd₆₇Au₃₃/C_II and Pd₅₀Au₅₀/C_II catalysts. Surface atomic ratios of Pd to Au in Pd₆₇Au₃₃/C_II and Pd₅₀Au₅₀/C_II are 67:33 and 52:48 respectively. The values are similar to the stoichiometric values of Pd₆₇Au₃₃/C_II (67:33) and Pd₅₀Au₅₀/C_II (50:50).

Fig. 10a shows CV of Pd/C, Au/C and Pd–Au/C catalysts with different metallic compositions in Ar saturated perchloric acid solution with a high upper limit potential (i.e., 1.6 V). The reduction

peaks of surface oxide on Pd/C and Au/C catalysts are at about 0.6 V and 1.17 V respectively, consistent with the literature report [25]. Two surface oxide reduction peaks are observed on Pd–Au/C catalysts, with one peak at Pd oxide reduction region (lower potential) and the other at Au oxide reduction region (higher potential). Large shift of reduction peaks on Pd–Au/C catalysts with different metallic compositions can be observed. Fig. 10b compares the peak potentials of the Pd–Au surface oxide reduction on different catalysts. Clearly, both of the two reduction peaks on each Pd–Au/C catalysts are between that of pure Pd and Au, which could indicate alloy structure of Pd–Au [25].

Fig. 11a compares the polarization curves (the oxidation currents were normalized by Pd contents characterized by ICP-AES) of formic acid oxidation on Pd/C and Pd–Au/C alloys with different metallic compositions. All carbon supported Pd–Au alloys exhibit higher Pd-mass activities compared with pure Pd. Fig. 11b compares the Pd-specific activities of Pd–Au catalysts with different metallic compositions for formic acid oxidation at 0.2 V. Clearly, the Pd-specific activities are higher on catalysts with higher content of Au. Interestingly, a shift of sharp current increase in the backward sweep was observed on catalysts with different metallic compositions. Larger shift towards more positive potential was clearly observed on Pd–Au catalysts with higher content of Au (Fig. 11a and c), suggesting an easier removal of adsorbed oxygen species from Pd–Au alloy catalysts with higher content of Au. Consistent with the previous discussion (Section 3.2), the higher alloying component of Au on Pd contributes to the easier removal of adsorbed oxygen species from Pd–Au alloy surface.

4. Conclusions

A simple co-deposition strategy for the synthesis of carbon-supported Pd–Au alloy was developed. This approach involves the co-reduction of Au and Pd ions in a controlled environment of ethylene glycol and sodium citrate as the reducing and stabilizing reagents. Both alloy and non-alloy Pd–Au nanoparticles could be achieved by choosing the right rate-limiting reactant during the reduction process. Higher Pd-specific activity was achieved on Pd–Au alloy catalyst compared with the non-alloy counterpart or its individual component, e.g., Pd. Easier removal of adsorbed oxygen species from Pd–Au alloy with a higher content of Au was observed.

Acknowledgements

The authors gratefully acknowledge the Research Grants Council of the Hong Kong SAR Government for the funding support. The postgraduate scholarship to Yange Suo from the Nanoscience and Nanotechnology program of School of Engineering is also appreciated. Technical support on surface analysis from the staff of Materials Characterization and Preparation Facility (MCPF) of HKUST is also appreciated.

References

- [1] J. Zhang, K. Sasaki, E. Sutter, R.R. Adzic, *Science* 315 (2007) 220.
- [2] Y.G. Suo, L. Zhuang, J.T. Lu, *Angew. Chem. Int. Ed.* 46 (2007) 2862.
- [3] Y. Mizukoshi, T. Fujimoto, Y. Nagata, R. Oshima, Y. Maeda, *J. Phys. Chem. B* 104 (2000) 6028.
- [4] M.S. Chen, D. Kumar, C.W. Yi, D.W. Goodman, *Science* 310 (2005) 291.
- [5] D.I. Enache, J.K. Edwards, P. Landon, B. Solsona-Espriu, A.F. Carley, A.A. Herzog, M. Watanabe, C.J. Kiely, D.W. Knight, G.J. Hutchings, *Science* 311 (2006) 362.
- [6] F. Ksar, L. Ramos, B. Keita, L. Nadjo, P. Beauvier, H. Remita, *Chem. Mater.* 21 (2009) 3677.
- [7] C.W. Xu, Z.Q. Tian, Z.C. Chen, S.P. Jiang, *Electrochem. Commun.* 10 (2008) 246.
- [8] W.J. Zhou, J.Y. Lee, *Electrochem. Commun.* 9 (2007) 1725.
- [9] I.-S. Park, K.-S. Lee, S.J. Yoo, Y.-H. Cho, Y.-E. Sung, *Electrochim. Acta* 55 (2010) 4339.
- [10] S. Alayoglu, A.U. Nilekar, M. Mavrikakis, B. Eichhorn, *Nat. Mater.* 7 (2008) 333.

- [11] R. Harpeness, A. Gedanken, *Langmuir* 20 (2004) 3431.
- [12] Y.W. Lee, M. Kim, Z.H. Kim, S.W. Han, *J. Am. Chem. Soc.* 131 (2009) 17036.
- [13] A. Henglein, *J. Phys. Chem. B* 104 (2000) 6683.
- [14] J.W. Hu, J.F. Li, B. Ren, D.Y. Wu, S.G. Sun, Z.Q. Tian, *J. Phys. Chem. C* 111 (2007) 1105.
- [15] S. Nath, S. Praharaj, S. Panigrahi, S.K. Ghosh, S. Kundu, S. Basu, T. Pal, *Langmuir* 21 (2005) 10405.
- [16] S.J. Mejia-Rosales, C. Fernández-Navarro, E. Pérez-Tijerina, D.A. Blom, L.F. Allard, M. José-Yacamán, *J. Phys. Chem. C* 111 (2007) 1256.
- [17] Y.W. Lee, M. Kim, Y. Kim, S.W. Kang, J.H. Lee, S.W. Han, *J. Phys. Chem. C* 114 (2010) 7689.
- [18] R. Jenkins, R.L. Snyder, *Introduction to X-ray Powder Diffractometry*, Wiley, New York, 1996.
- [19] A.R. Denton, N.W. Ashcroft, *Phys. Rev. A* 43 (1991) 3161.
- [20] M.S. Antelman, F.J. Harris, *The Encyclopedia of Chemical Electrode Potentials*, Plenum Press, New York, 1982.
- [21] X. Li, Xi. Qiu, H. Yuan, L. Chen, W. Zhu, *J. Power Sources* 184 (2008) 353.
- [22] Y. Suo, I.M. Hsing, *Electrochim. Acta* 55 (2009) 210.
- [23] B. Hammer, J.K. Nørskov, *Surf. Sci.* 343 (1995) 211.
- [24] J. Greeley, J.K. Nørskov, *Surf. Sci.* 592 (2005) 104.
- [25] F.A. Al-Odail, A. Anastasopoulos, B.E. Hayden, *Phys. Chem. Chem. Phys.* 12 (2010) 11398.